

# The Compton shoulder of the Fe K $\alpha$ fluorescent emission line in active galactic nuclei

Tahir Yaqoob<sup>1</sup> and Kendrah D. Murphy<sup>2,3</sup>

<sup>1</sup>*Department of Physics and Astronomy, Johns Hopkins University, Baltimore, MD 21218.*

<sup>2</sup>*MIT Kavli Institute for Astrophysics and Space Research, 77 Massachusetts Avenue, NE80-6013, Cambridge, MA 02139.*

<sup>3</sup>*Department of Physics, Skidmore College, 815 North Broadway, Saratoga Springs, NY 12866.*

Accepted. Received; in original form

## ABSTRACT

We present new, high signal-to-noise ratio results from a Monte Carlo study of the properties of the Compton shoulder of the Fe K $\alpha$  emission line in the toroidal X-ray reprocessor model of Murphy & Yaqoob (2009). The model is valid for equatorial column densities in the range  $10^{22}$  cm<sup>-2</sup> to  $10^{25}$  cm<sup>-2</sup>, which comprehensively covers the Compton-thin to Compton-thick regimes. We show how the shape of the Compton shoulder and its flux relative to the core of the Fe K $\alpha$  emission line depend on the torus column density and orientation, for the case of a half-opening angle of 60° and cosmic abundances. The variety of Compton shoulder profiles is greater than that for both (centrally-illuminated) spherical and disk geometries. Our Monte Carlo simulations were done with a statistical accuracy that is high enough to reveal, for the case of an edge-on, Compton-thick torus, a new type of Compton shoulder that is not present in the spherical or disk geometries. Such a Compton shoulder is dominated by a narrow back-scattering feature peaking at  $\sim 6.24$  keV. Our results are also sensitive enough to reveal a dependence of the shape of the Compton shoulder (and its magnitude relative to the Fe K $\alpha$  line core) on the spectral shape of the incident X-ray continuum. We also present results of the effect of velocity broadening on the Fe K $\alpha$  line profile and find that if either the velocity width or instrument resolution is greater than a FWHM of  $\sim 2000$  km s<sup>-1</sup>, the Compton shoulder begins to become blended with the line core and the characteristic features of the Compton shoulder become harder to resolve. In particular, at a FWHM of  $\sim 7000$  km s<sup>-1</sup> the Compton shoulder is not resolved at all, its only signature being a weak asymmetry in the blended line profile. This means that CCD X-ray detectors cannot unambiguously resolve the Compton shoulder. Our results are freely available in a format that is suitable for direct spectral-fitting of the continuum and line model to real data.

**Keywords:** galaxies: active - line:formation - radiation mechanism: general - scattering - X-rays: general

## 1 INTRODUCTION

The narrow Fe K $\alpha$  emission line in Active Galactic Nuclei (AGNs) is by now an established feature of the X-ray spectrum of both type 1 and type 2 sources (e.g. see Shu, Yaqoob, & Wang 2010, and references therein). The FWHM of the emission line is usually found to be less than  $\sim 5000$  km s<sup>-1</sup> or so, indicating an origin in the outer (optical) broad line region (BLR) or further out, in the putative parsec-scale torus (e.g. Yaqoob & Padmanabhan 2004; Bianchi et al. 2008; Shu et al. 2010). From a subsample of the highest quality *Chandra* HETG spectra, Shu et al. (2010) in fact found that the width of the Fe K $\alpha$  line relative to the optical line width of H $\beta$  varies from source to source so that there may not be a “universal” location for the X-ray reprocessor. X-ray spectroscopy also shows overwhelming evidence for the Fe K $\alpha$  line peaking at  $\sim 6.4$  keV, indicating that the matter responsible for producing this line is essentially neutral (e.g. Sulentic et al. 1998; Weaver, Gelbord, & Yaqoob 2001; Reeves 2003; Page et al. 2004; Yaqoob & Padmanabhan 2004; Jiménez-Bailón et al. 2005; Zhou & Wang

2005; Jiang, Wang, & Wang 2006; Levenson et al. 2006; Shu et al. 2010). Although emission lines from ionized species of Fe are observed in some AGN (e.g. Yaqoob et al. 2003; Bianchi et al. 2005, 2008), the present paper is concerned specifically with the Fe  $K\alpha$  line component that is centered around 6.4 keV. Although some type 2 AGN do not show evidence for line-of-sight X-ray obscuration (Brightman & Nandra 2008), in general the “type classification” of AGN appears to be related to the orientation of the structure of circumnuclear matter in the central engine. This, along with the fact that the narrow Fe  $K\alpha$  line at  $\sim 6.4$  keV appears in the X-ray spectra of AGN regardless of whether or not the X-ray spectrum shows line-of-sight obscuration suggests that the material producing the Fe  $K\alpha$  emission line is in some sense toroidal.

The modification of the intrinsic X-ray spectrum due to the effects of absorption, scattering and fluorescence in the circumnuclear matter are not trivial to calculate in the Compton-thick regime since the reprocessing is a complicated function of column density, geometry (and covering factor), element abundances, and the system inclination angle (e.g. Ghisellini, Haardt, & Matt 1994; Ikeda, Awaki, & Terashima 2009). To obtain the most accurate spectra, Monte Carlo simulations are required. In Murphy & Yaqoob (2009, hereafter MY09) and Yaqoob et al. (2010) we presented the results of Monte Carlo calculations for the reprocessed X-ray continuum and the Fe  $K\alpha$  emission line in a toroidal geometry, valid for column densities in the range  $10^{22}$  to  $10^{25}$   $\text{cm}^{-2}$ , thus covering the Compton-thin to Compton-thick regimes. Only the results for the zeroth-order, or core, component for the Fe  $K\alpha$  emission line in the MY09 model have been presented thus far (the zeroth-order component corresponds to line photons that escape the medium without scattering). The scattered emission-line photons constitute the so-called “Compton shoulder”, which can provide additional critical information on the column density and orientation of the line emitter (e.g. Ghisellini et al. 1994; Sunyaev & Churazov 1996; Matt 2002; Watanabe et al. 2003). Given the high degree of degeneracy in modeling complex X-ray spectra, including a physical model of the Compton shoulder (as opposed to a simple ad hoc component) is important, especially in view of the fact that even the non-detection of a Compton shoulder provides constraints on the physical parameters of the model. Quantifying upper limits on the Compton shoulder when it is not detected particularly demands a physically-motivated model. We have substantially improved the statistical accuracy of the X-ray spectra of the toroidal reprocessor model (MYTORUS) described in MY09 in order for it to be suitable for spectral-fitting to real data. The Monte Carlo results have been put into formats that are readily useable in conjunction with standard X-ray spectral-fitting packages and we have made the MYTORUS model publicly available<sup>1</sup>. In the present paper we describe the detailed form of the Compton shoulder of the Fe  $K\alpha$  line in a toroidal geometry and discuss its dependence on the model parameters.

We note that the MYTORUS model is not restricted to any absolute size scale so it can be applied to *any* toroidal distribution of matter that is centrally-illuminated by X-rays. Gaskell, Goosmann, & Klimek (2008) argue that there is considerable observational evidence that the BLR itself has a toroidal structure, and that there may be no distinct boundary between the BLR and the classical parsec-scale torus. Gaskell et al. (2008) also argue that there may even be no distinction between the outer accretion disk and the BLR. A toroidal distribution of matter may exist anywhere from the outer accretion disk to parsec-scale distances from the X-ray continuum source. Thus, throughout the present paper, we shall refer to *ANY* toroidal distribution of matter in the central engine as “the torus”, regardless of its actual size or physical location in the AGN central engine. Our torus model complements hydrodynamical, photoionized *torus wind* simulations such as those of Dorodnitsyn & Kallman (2009) which are designed to account for the emission lines from ionized species in AGN, and the photoionized absorber and emission lines from ionized in some type 1 AGN. Such models of evaporation of the inner torus do not account for the Fe  $K\alpha$  line component that is centered around  $\sim 6.4$  keV, which must originate in the cooler, unionized region of the torus.

The paper is organized as follows. In §2 we give a brief overview of the assumptions of the MYTORUS model and in §3 we clarify the definition of the Fe  $K\alpha$  line Compton shoulder in the present paper. In §4 we present the results for the ratio of the Fe  $K\alpha$  line Compton shoulder flux to the zeroth-order flux, and in §5 we discuss the characteristic shapes of the Compton shoulder profile as a function of some of the model parameters. In §6 we illustrate the dependence of the shape of the Compton shoulder profile on the form of the intrinsic, incident X-ray continuum, and in §7 we discuss the effects of velocity broadening on the Fe  $K\alpha$  line core and Compton shoulder. We summarize our conclusions in §8.

## 2 OVERVIEW OF MODEL ASSUMPTIONS

Here we give a brief overview of the critical assumptions that the model Monte Carlo simulations are based upon. Full details can be found in MY09. Our geometry is an azimuthally-symmetric doughnut-like torus with a circular cross-section, characterized by only two parameters, namely the half-opening angle,  $\theta_0$ , and the equatorial column density,  $N_H$  (see Fig. 1 in MY09). We assume that the X-ray source is located at the center of the torus and emits isotropically and that the reprocessing material is uniform and essentially neutral (cold). For illumination by an X-ray source that is emitting isotropically, the mean column density, integrated over all incident angles of rays through the torus, is  $\bar{N}_H = (\pi/4)N_H$ . The inclination angle between

<sup>1</sup> See <http://www.mytorus.com>

the observer’s line of sight and the symmetry axis of the torus is denoted by  $\theta_{\text{obs}}$ , where  $\theta_{\text{obs}} = 0^\circ$  corresponds to a face-on observing angle and  $\theta_{\text{obs}} = 90^\circ$  corresponds to an edge-on observing angle. In our calculations we distribute the emergent photons in 10 angle bins between  $0^\circ$  and  $90^\circ$  that have equal widths in  $\cos\theta_{\text{obs}}$ , and refer to the face-on bin as #1, and the edge-on bin as #10 (see Table 1 in MY09).

The value of  $\theta_0$  for which we have calculated a comprehensive set of models is  $60^\circ$ , for  $N_H$  in the range  $10^{22}$  cm $^{-2}$  to  $10^{25}$  cm $^{-2}$ , valid for input spectra with energies in the range 0.5–500 keV (see MY09 for details). For  $\theta_0 = 60^\circ$ , the solid angle subtended by the torus at the X-ray source,  $\Delta\Omega$ , is  $2\pi$  (and we refer to  $[\Delta\Omega/(4\pi)]$  as a covering factor, which in this case is 0.5). The covering factor may also be expressed in terms of the physical dimensions of the torus. If  $a$  is the radius of the circular cross-section of the torus, and  $c + a$  is the equatorial (i.e. maximum) radius of the torus then  $[\Delta\Omega/(4\pi)] = (a/c)$  (see MY09). Our model employs a full relativistic treatment of Compton scattering, using the full differential and total Klein-Nishina Compton-scattering cross-sections. We utilized photoelectric absorption cross-sections for 30 elements as described in Verner & Yakovlev (1995) and Verner et al. (1996) and we used Anders and Grevesse (1989) elemental cosmic abundances in our calculations. The Thomson depth may also be expressed in terms of the column density:  $\tau_T = KN_H\sigma_T \sim 0.809N_{24}$  where  $N_{24}$  is the column density in units of  $10^{24}$  cm $^{-2}$ . Here, we have employed the mean number of electrons per H atom,  $\frac{1}{2}(1 + \mu)$ , where  $\mu$  is the mean molecular weight. With the abundances of Anders & Grevesse,  $K = 1.21656$ , assuming that the number of electrons from all other elements aside from H and He is negligible. For the Fe K $\alpha$  and Fe K $\beta$  fluorescent emission lines, we used rest-frame line energies of 6.4008 keV and 7.058 keV respectively, appropriate for neutral matter (e.g. see Palmeri et al. 2003). We used a fluorescence yield for Fe of 0.347 (see Bambynek et al. 1972) and an Fe K $\beta$  to Fe K $\alpha$  branching ratio of 0.135 (representative of the range of experimental and theoretical values discussed in Palmeri et al. 2003, see also Kallman et al. 2004).

Compared to MY09, the results in the present paper have a substantially higher statistical accuracy because they are based on Monte Carlo simulations with higher numbers of injected rays at each energy, and the calculations employ the method of weights (as opposed to following individual photons). The statistical accuracy actually achieved depends on the model parameters. The most challenging regime corresponds to the highest column density torus ( $10^{25}$  cm $^{-2}$ ) observed edge-on, and in this worst-case scenario the statistical errors on the Compton shoulder profile (for the default torus opening angle and abundances) are better than 2% per 100 eV energy bin. On the other hand, for a face-on torus with a column density of  $10^{24}$  cm $^{-2}$ , the corresponding statistical errors on the Compton shoulder profile are better than 0.2% per 100 eV bin.

Throughout the present paper we present results for power-law incident continua (in the range 0.5–500 keV), characterized by a photon index,  $\Gamma$ , by integrating the basic monoenergetic Monte Carlo results (Greens functions– see MY09).

### 3 DEFINITION OF THE Fe K $\alpha$ LINE COMPTON SHOULDER

The zeroth-order component of the Fe K $\alpha$  fluorescent emission line refers to line photons that escape without any interaction with the medium that they were created in. Although they are emitted by atoms/ions isotropically, the angular distribution of the emerging zeroth-order line photons in general depends on the geometry, unless the medium is optically-thin to the line photons. The zeroth-order line photons constitute the majority of photons in the emergent emission line for the parameters pertaining to our model assumptions, and they all have the same energy in the Monte Carlo results because they have not interacted with the medium. When velocity broadening is applied to the zeroth-order line emission the photon energies are of course modified to reflect the distribution of the broadening function. Most of the fluorescent Fe K $\alpha$  emission-line measurements in the literature that have been modeled with simple Gaussian functions correspond to the zeroth-order of the emission line. However, depending on the spectral resolution of the instrument, some of the measured flux of this line core may include a contribution from the Compton-scattered line photons (or Compton shoulder) since the scattered line component consists of photons with a range of energies going all the way up to the zeroth-order line energy. If one compares the results of applying the MYTORUS model to results in the literature that were obtained using ad hoc models for the Fe K $\alpha$  line core and Compton shoulder one must scrutinize precisely which components of the line were actually measured with the ad hoc model components.

We refer to fluorescent emission-line photons that escape the medium after at least one interaction as the scattered component of the line. Compton scattering shapes the energy distribution of the scattered line photons. However, the final scattered line profile depends on the geometry, orientation, and column density distribution of the medium because the escape probabilities after scattering may be highly directional. In cold matter, the scattered photon distribution resulting from the  $n$ th scattering has a spread in energy from  $E_0$  (the rest-frame zeroth-order line energy), down to  $511/[(511/E_0 \text{ keV}) + 2n]$  keV. The number of photons in each scattering order is diminished compared to the number in the previous scattering order. The exact dependence of the relative number of photons in each scattering, and therefore of the measurable width of the scattered distribution, is a function of model parameters. If the optical depth to absorption of the line photons is much greater or much less than unity, only the first scattering may dominate. Even for intermediate optical depths the third scattering is, for practical purposes, negligible in flux compared to the first scattering.

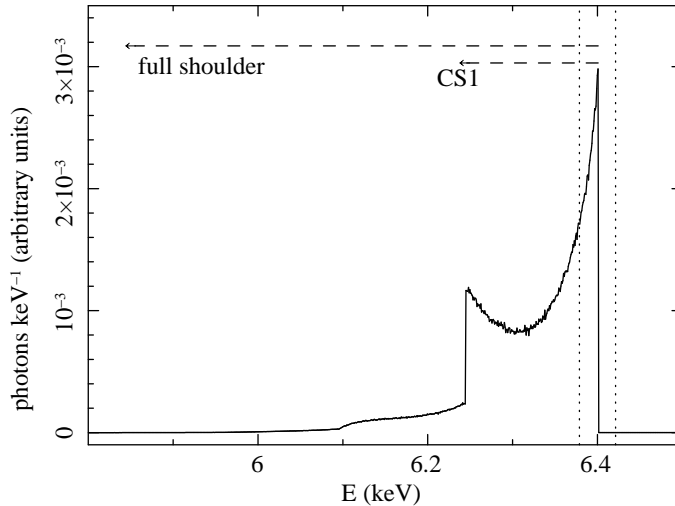


**Figure 1.** Illustration of our definition of the Compton shoulder for an emission line, compared with the definition “CS1”. Our definition (“full shoulder” in the figure) includes ALL of the scattered line flux, but “CS1” includes all of the flux only in the energy interval of the first scattering. Note that no velocity broadening has been applied. When velocity broadening is applied, ad hoc models will confuse line flux from the zeroth-order and the Compton shoulder (regardless of definition). The vertical dotted lines in the figure illustrate this by showing the energy width corresponding to  $\pm 1000 \text{ km s}^{-1}$  either side of the zeroth-order line energy.

The term “Compton shoulder” has been used in the literature in more than one way. The most common usage refers to the line flux between the energy extrema of the first scattering, *which includes some contributions from all scatterings*. This is because the contributions from all scattering orders extends to the zeroth-order line energy and different scattering orders cannot be measured separately. This is referred to as “CS1” (e.g. see Matt 2002), and is illustrated in Fig. 1. Some literature may refer to only the first scattering as the Compton shoulder, but this of course can only have a theoretical context. A third definition, which is the one we use here and throughout the present paper, is that the Compton shoulder includes *all* of the scattered line flux, for all scatterings (see Fig. 1). This is the most appropriate definition for a model such as MYTORUS which self-consistently calculates the zeroth-order and the entire scattered line profile and does not allow the relative fluxes of the two components to vary in an ad hoc fashion. Definitions such as CS1 are not necessary for our purpose because there is no need to fit the scattered component of an emission line separately.

In practice it may not actually be possible to observationally distinguish the zeroth-order component of an emission line from its Compton shoulder. The finite energy resolution of the instrument and/or the velocity broadening (of all the emission-line components) may confuse the two blended components of a line. This is illustrated in Fig. 1 with dotted lines placed at energies corresponding to  $\pm 1000 \text{ km s}^{-1}$  either side of the zeroth-order line energy. Having said that, one will never need to observationally distinguish between the zeroth-order component of an emission line from its Compton shoulder with the MYTORUS model because it is a self-consistent model. However, it is important to be aware of the “mixing” for the interpretation of spectral-fitting results, and more will be said on this topic when we discuss velocity broadening in §7.

#### 4 RELATIVE MAGNITUDE OF THE COMPTON SHOULDER

The relative magnitude of the zeroth-order and scattered line components is fixed by the physics and geometry and in Fig. 2 we show the ratio of the Fe  $K\alpha$  line Compton shoulder flux to the zeroth-order line flux (hereafter, the CS ratio) as a function of  $N_H$  for two different values of  $\theta_{\text{obs}}$  (corresponding to the face-on and edge-on inclination angle bins –see Table 1 in MY09). The calculations in Fig. 2 were made for an incident power-law continuum with a photon index of 1.9. It can be seen that the ratio peaks at  $N_H \sim 2 - 3 \times 10^{24} \text{ cm}^{-2}$ , reaching a maximum of  $\sim 0.29$  (face-on), and  $\sim 0.37$  (edge-on). For the face-on case, the CS ratio remains at  $\sim 0.29$  for higher column densities since the Compton shoulder photons escape from within a Compton-depth or so from the illuminated surfaces of the torus for lines-of-sight that are not obscured. For the edge-on case the CS ratio declines as function of column density after reaching its maximum value, due to a higher probability of absorption at higher column densities. In the optically-thin limit, one might expect the CS ratio to be approximately  $\sim K\sigma_T(\pi/4)N_H = 0.809(\pi/4)N_{24}$ , and this relation is shown in Fig. 2 (dotted line). The actual CS ratios fall below this line because the Fe  $K\alpha$  line photons are formed throughout the medium, so that the average column density for scattering of the line photons is less than  $(\pi/4)N_H$ . At  $N_H = 10^{22} \text{ cm}^{-2}$ , the CS ratio is a factor  $\sim 0.80$ , and  $\sim 0.87$  less than  $0.809(\pi/4)N_{24}$  for the face-on and edge-on orientation respectively. The face-on orientation obviously has a smaller mean column density than the edge-on one.

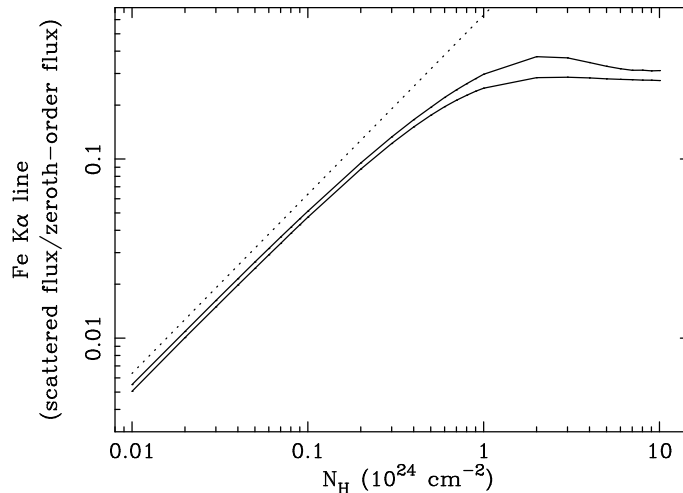


**Figure 2.** The ratio of the scattered flux to the zeroth-order flux in the Fe  $K\alpha$  line from the MYTORUS model, as a function of  $N_H$  (for  $\Gamma = 1.9$ ). Shown are curves for the face-on (lower curve) and edge-on (upper curve) inclination-angle bins. The dotted curve corresponds to a CS ratio of  $0.809(\pi/4)N_{24}$  in order to compare with the Monte Carlo results in the optically-thin limit. See text in §4 for further details.

Matt (2002) showed the CS ratio for spherical and disk geometries (albeit for the “CS1” definition of the Compton shoulder). The spherical geometry shows a maximum CS ratio of  $\sim 0.42$  for  $N_H \sim 2 \times 10^{24} \text{ cm}^{-2}$ , similar to the case for the edge-on torus (and note that the spherical radial column densities should be compared with  $\sim (\pi/4)$  times our equatorial torus column densities). The Compton-thick disk geometry shows a lower CS ratio, peaking at  $\sim 0.2$  (Matt 2002), less than the corresponding value for the Compton-thick face-on torus. The range of incident and emergent photon angles are very different for the two geometries and the differences in the reflection spectra from the torus and disk geometries have been discussed in MY09.

We found that for all values of  $\theta_{\text{obs}}$  for the torus, there was no detectable difference in the CS ratio as a function of  $\Gamma$  up to the  $N_H$  value that gives the maximum CS ratio (for a given value of  $\theta_{\text{obs}}$ ). After that, the CS ratios diverge for different values of  $\Gamma$ , with flatter incident continua giving larger CS ratios. For the face-on case, the CS ratio at  $N_H = 10^{25} \text{ cm}^{-2}$  varies between  $\sim 0.30$  to  $\sim 0.32$  as  $\Gamma$  varies from 2.5 to 1.5. For the edge-on case, the CS ratio at  $N_H = 10^{25} \text{ cm}^{-2}$  varies between  $\sim 0.28$  to  $\sim 0.27$  as  $\Gamma$  varies from 2.5 to 1.5. Flatter spectra have relatively more continuum photons at higher energies so that the Fe  $K\alpha$  line photons are produced deeper in the medium, increasing the average Thomson depth for zeroth-order line photons to scatter before escaping. Although these variations in the CS ratio with  $\Gamma$  are small, the effect of different values of  $\Gamma$  on the Compton shoulder *shape* is much more pronounced (see §6).

## 5 THE SHAPE OF THE COMPTON SHOULDER

The shape of the Compton shoulder of a fluorescent emission-line escaping from the torus has a dependence on the column density and inclination angle of the torus. It is also affected by the shape of the incident continuum spectrum, the covering factor (or opening angle), and element abundances. In this section we discuss the shape of the Fe  $K\alpha$  line shoulder for the default covering factor ( $[a/c] = 0.5$ ) and solar abundances. Fig. 3 and Fig. 4 illustrate the shapes of the Compton shoulder for a power-law incident continuum with  $\Gamma = 1.9$ , for four column densities ( $10^{23}$ ,  $10^{24}$ ,  $5 \times 10^{24}$ , and  $10^{25} \text{ cm}^{-2}$ ) and different inclination angles of the torus. Fig. 3 and Fig. 4 show Compton shoulders for the same physical parameters except that in the former the profiles are plotted against Compton wavelength shift and in the latter they are plotted against absolute energy. The Compton shoulders in Fig. 3 are in units of the *dimensionless* Compton wavelength shift with respect to the zeroth-order rest-frame energy of the emission line. In other words, if  $E$  is the energy of a line photon, and  $E_0$  is the zeroth-order line energy,  $\Delta\lambda = (511 \text{ keV}/E) - (511 \text{ keV}/E_0)$ . The Compton shoulder shapes shown in both Fig. 3 and Fig. 4 are from the original Monte Carlo results and have no velocity broadening applied to them. In order to facilitate a direct comparison of the Compton shoulder profile shapes for different column densities and inclination angles, all of the profiles in Fig. 3 have been normalized to a flux of unity. It should be remembered that the absolute flux of the Compton shoulder varies significantly with column density, and the flux ratio for two column densities can be estimated using Fig. 2. The Compton shoulder profiles that are plotted against energy (Fig. 4) *do* show *relative* fluxes for different parameters that reflect the original Monte Carlo results.

Interpretation of Fig. 3 is aided by the relation between  $\Delta\lambda$  and the scattering angle,  $\alpha$ :  $\Delta\lambda = 1 - \cos\alpha$ . We can see from Fig. 3 that at a column density of  $10^{23} \text{ cm}^{-2}$  the Compton shoulder is dominated by the first scattering and the profile

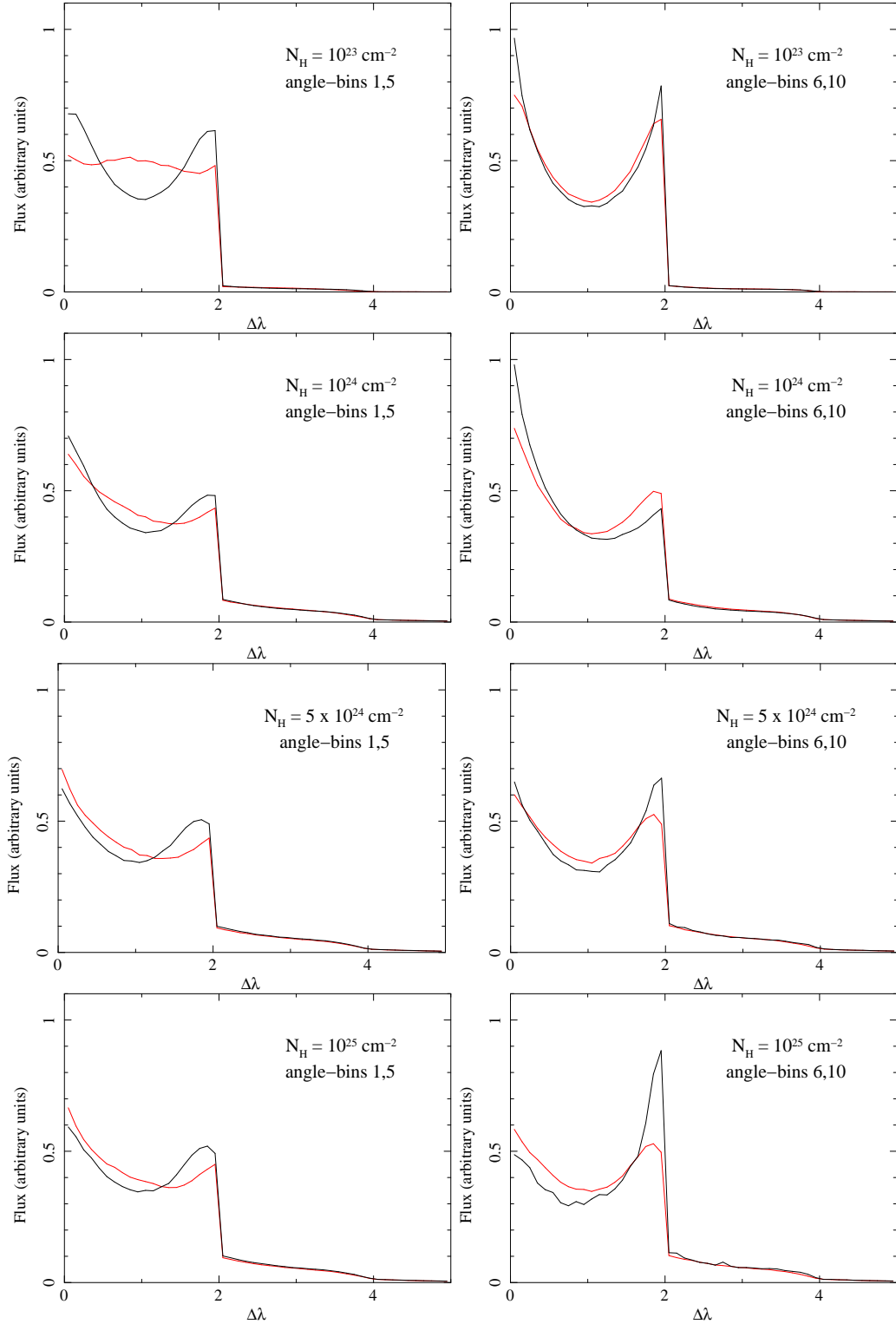


**Figure 3.** The Fe  $K\alpha$  emission-line Compton shoulders for a power-law incident continuum with  $\Gamma = 1.9$ , for four column densities (from top to bottom,  $N_{\text{H}} = 10^{23}$ ,  $10^{24}$ ,  $5 \times 10^{24}$ , and  $10^{25} \text{ cm}^{-2}$ ) and different inclination angles of the torus. The left-hand panels show the two extreme non-intercepting angle bins #1 (red) and #5 (black), and the right-hand panels show the two extreme intercepting angle bins, #6 (red) and #10 (black)– see Table 1 in MY09. No velocity broadening has been applied. *Note that in order to directly compare the Compton shoulder shapes, the total flux for each shoulder has been renormalized to the same value.* The line flux (in units of normalized flux per unit wavelength shift) is plotted against the dimensionless Compton wavelength shift with respect to the zeroth-order rest-frame energy of the emission line ( $E_0$ ),  $\Delta\lambda = (511 \text{ keV}/E) - (511 \text{ keV}/E_0)$ .

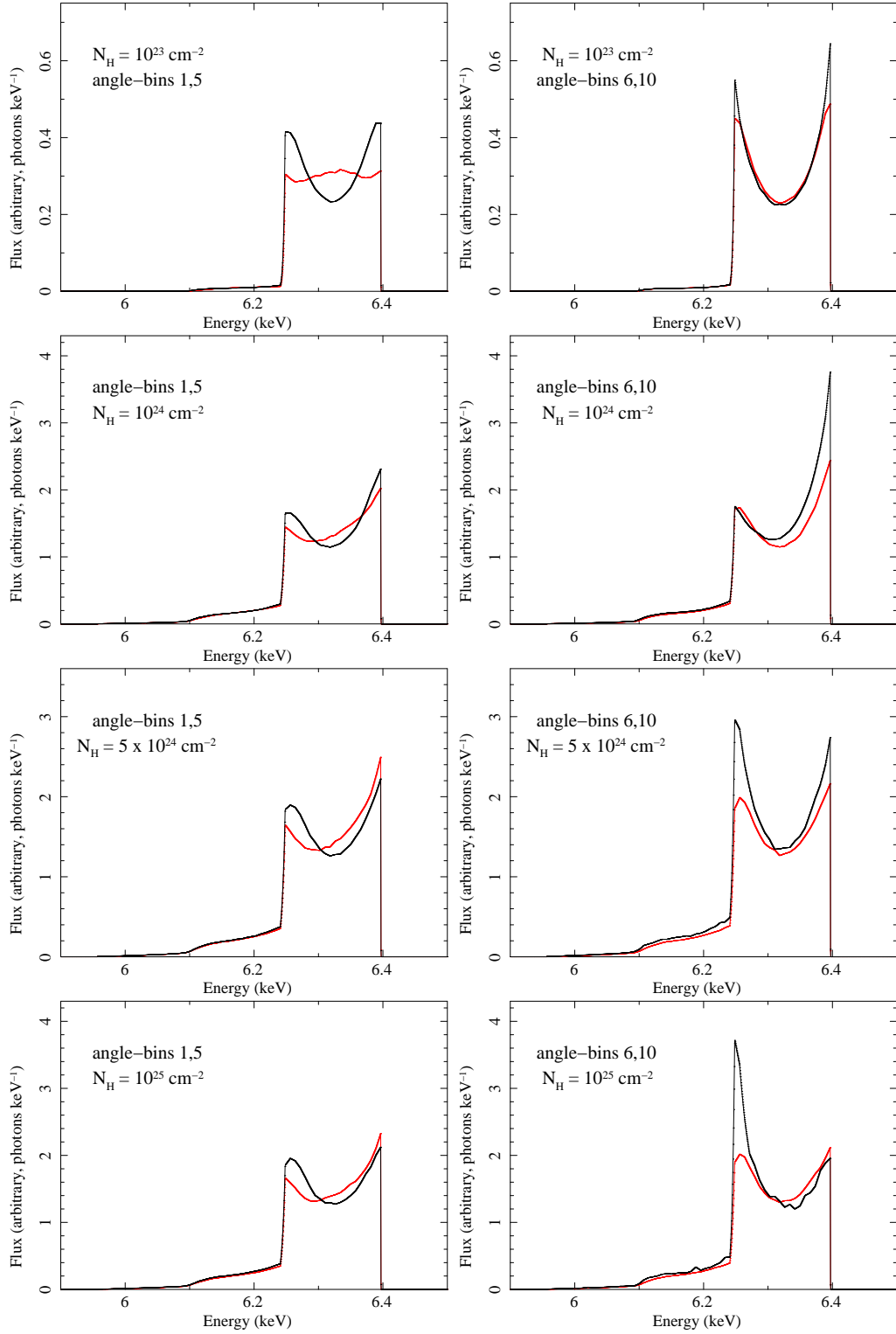


**Figure 4.** The Fe  $K\alpha$  emission-line Compton shoulders for a power-law incident continuum with  $\Gamma = 1.9$ , for four column densities (from top to bottom,  $N_{\text{H}} = 10^{23}$ ,  $10^{24}$ ,  $5 \times 10^{24}$ , and  $10^{25} \text{ cm}^{-2}$ ) and different inclination angles of the torus. The left-hand panels show the two extreme non-intercepting angle bins #1 (red) and #5 (black), and the right-hand panels show the two extreme intercepting angle bins, #6 (red) and #10 (black)– see Table 1 in MY09. No velocity broadening has been applied. The Compton shoulders correspond to identical parameters to those in Fig. 3, but here the profiles are plotted against energy and the units of flux are photons  $\text{keV}^{-1}$ . Although the overall absolute normalization is arbitrary, the Compton shoulder profiles have relative normalizations that reflect the original Monte Carlo results.

is determined by the appropriate sampling of the single-scattering Thomson differential cross-section (which is peaked for forward and backward scattering and has a minimum for orthogonal scattering angles). For the face-on Compton shoulder at such low column densities, the forward and backward scattering peaks are suppressed, giving an essentially flat Compton shoulder profile. This is because most of the scattering occurs in the equatorial plane of the torus when the scattering optical depth is small because the equatorial plane presents the largest column density. Thus, zeroth-order line photons with directions that roughly align with the equatorial plane must scatter predominantly at right angles in order to be observed in the face-on torus  $\theta_{\text{obs}}$  bin. On the other hand, those zeroth-order line photons that undergo forward and backward scattering are likely to be traveling in directions aligned with the equatorial plane again after scattering so are not as likely to appear in the face-on torus  $\theta_{\text{obs}}$  bin. For larger inclination angles, we see in Fig. 3 that the forward and backward scattering peaks become more and more prominent, and for the edge-on angle bin they are significantly enhanced and the  $90^\circ$  scattering direction is correspondingly suppressed. We obtained similar Compton shoulder profiles for column densities less than  $10^{23} \text{ cm}^{-2}$ .

As the column density of the torus increases, a scattered line photon is more likely to escape the medium if it scatters near a surface. Near the non-illuminated surfaces of the torus (i.e. the surfaces with more material in between the X-ray source and the first scattering), there are less zeroth-order Fe  $K\alpha$  line photons produced. The zeroth-order line photons that do appear near the far-side surfaces were more likely produced near an illuminated surface and are therefore predominantly heading *towards* the far surface rather than away from it. However, even if a zeroth-order line photon is traveling towards the surface (no matter how far from the X-ray source), if it is back-scattered, the scattered photon then travels back in to the medium, with a higher mean free path to escape. Therefore, the scattered photons that are produced by zeroth-order line photons traveling towards the surface *and* undergo forward scattering will preferentially escape the medium. We can see this in Fig. 3 for  $N_H = 10^{24} \text{ cm}^{-2}$ , which shows enhancement of the forward-scattering peak and suppression of the back-scattering peak. The effect is more and more pronounced as the inclination angle becomes larger and larger because back-scattered photons could be intercepted by the other side of the torus, presenting a large mean free path to escape compared to photons back-scattering near the surface in directions perpendicular to the equatorial plane. Also, the parts of the torus that scatter line photons into non-intercepting lines of sight present a mean column density to the X-ray continuum that is smaller than the equatorial parts of the torus. Thus, the edge-on Compton shoulder profiles for  $N_H = 10^{24} \text{ cm}^{-2}$  are significantly asymmetric, weighted in favor of forward-scattering.

As the column density of the torus increases even further, the zeroth-order Fe  $K\alpha$  line photons are created closer and closer to the surfaces nearest the continuum illumination since the continuum flux that produces the fluorescence diminishes further into the medium. Therefore scattered photons preferentially escape from the illuminated surfaces. Thus, the probability of scattered photons escaping from the medium is not very different for forward-scattering and back-scattering because now there is no selection effect for the original zeroth-order line photon to be heading towards a surface before scattering. At lower column densities, zeroth-order photons could end up a longer way into the medium, far from an illuminated surface, where it was less unlikely to find a zeroth-order photon traveling *away* from the surface (in which case it would have to back-scatter to escape). However, now for a higher column density, there is a dearth of zeroth-order line photons near surfaces that are not directly illuminated by the continuum because large numbers are absorbed or scattered before they get there, and the continuum is heavily extinguished, producing less zeroth-order photons near far-side surfaces. It can be seen from Fig. 3 that for  $N_H = 5 \times 10^{24} \text{ cm}^{-2}$ , the forward-scattering peak is now indeed not particularly strong compared to the back-scattering peak and the Compton shoulder profiles have now become more symmetric again for the intercepting lines of sight. Some of this symmetry is caused by the higher-order scatterings effectively raising the back-scattering peak. The Compton shoulder profiles for the non-intercepting lines-of-sight are not very different to those for  $N_H = 10^{24} \text{ cm}^{-2}$  (i.e they still have a slightly higher weighting on the forward-scattering peak). This is because for these scattered photons no material is being added between the observer and the scattering sites as the column density increases, and adding more optical depth deeper in the medium does not make much difference because the deeper scattering sites cannot make a further significant contribution to the observed scattered flux.

Now, moving on to the highest column density Compton shoulder profiles in Fig. 3 ( $10^{25} \text{ cm}^{-2}$ ) we see that those for the non-intercepting lines-of-sight are essentially similar to those for a column density of  $5 \times 10^{24} \text{ cm}^{-2}$ . This is not surprising because the medium was already Compton thick at that column density and the Compton shoulder photons were already dominated by scattering near the illuminated surfaces, with clear lines-of-sight to the observer. However, the situation is different as we go to an edge-on orientation of the torus. Here we see that it is the *back-scattering* peak that now dominates over the forward-scattering peak. The reason for this is that most of the torus is so Compton-thick that all of the Compton shoulder photons now come from two “rings” on opposite surfaces of the torus, such that the rings are regions having the smallest column density in directions parallel to the equatorial plane. For zeroth-order line photons that are created and scattered in this band of emission, there is no preference for forward and backward-scattering. However, it is possible that zeroth-order line photons that escaped from the inner surface of the torus closer to the equatorial plane, can scatter in the “ring” and be observed in the Compton shoulder profile. For the smaller column density of  $5 \times 10^{24} \text{ cm}^{-2}$  these photons could forward-scatter or backward-scatter in the “ring” and still reach the observer. However, at a column density of  $10^{25} \text{ cm}^{-2}$  the opacity is so high for the forward-scattering route that it is suppressed. The backward-scattering route on the other



hand, does not have to intercept the other side of the torus again before escape, unless the line-of-sight is *exactly* edge-on. Recall that our edge-on angle bin is actually a wedge that is a few degrees wide (see Table 1 in MY09). Thus, for an exactly edge-on orientation, the back-scattering peak would again be suppressed. On the other hand, if the torus is actually patchy (for example, consisting of a distribution of clouds), the back-scattering peak would be observed even for exactly edge-on orientations.

The profile in Fig. 3 (and in Fig. 4) for the edge-on case for  $N_H = 10^{25} \text{ cm}^{-2}$  is a *new*, type of Compton shoulder that has not been predicted before. It does not appear in spherical or disk geometries (e.g. George & Fabian 1991; Sunyaev & Churazov 1996; Matt 2002), and to reveal it in a toroidal geometry requires very high signal-to-noise Monte Carlo simulations, otherwise it is not discernible from the noise. In energy space, this type of Compton shoulder would show up in the X-ray spectrum as a peak at  $\sim 6.24 \text{ keV}$ , separated from the zeroth-order Fe  $K\alpha$  line core at  $\sim 6.4 \text{ keV}$  if the velocity width is small enough. If such a Compton shoulder were observed, it would be a powerful indicator of a toroidal structure (possibly made of discrete clumps) with a column density of the order of  $10^{25} \text{ cm}^{-2}$ , observed edge-on. In contrast, a centrally-illuminated, uniform spherical geometry does not have any non-intercepting lines of sight so it can only produce Compton shoulder profiles in the Compton-thick regime that are weighted towards forward scattering. Moreover, an externally illuminated Compton-thick disk *only* has non-intercepting lines of sight and can therefore only produce essentially symmetric Compton shoulder profiles, with no preference for forward or backward scattering.

## 6 DEPENDENCE OF THE COMPTON SHOULDER ON THE ILLUMINATING CONTINUUM

In §4 we reported a weak dependence of the ratio of the flux in the Compton shoulder to the zeroth-order Fe  $K\alpha$  line flux on the photon index,  $\Gamma$ , of the power-law incident continuum. Here we report the dependence of the *shape* of the Compton shoulder profile on  $\Gamma$ . Fig. 5 shows the Compton shoulder profiles for  $N_H = 10^{25} \text{ cm}^{-2}$ , directly comparing the cases of  $\Gamma = 1.5$  (dotted curves) and  $\Gamma = 2.5$  (solid curves) for face-on (*left panel*) and edge-on (*right panel*) orientations. As in Fig. 3 (and as described in §5), the fluxes have been renormalized so that the total flux is unity and the Compton shoulder profiles are plotted against  $\Delta\lambda$ . It can be seen that for the face-on orientation the dependence of the shape of the Compton shoulder profile on the steepness of the incident X-ray continuum is extremely weak and would not in practice be detectable. However, the situation is different for the edge-on orientation. The Compton shoulder profile is more symmetric for the flatter incident spectrum ( $\Gamma = 1.5$ ), whilst the steeper spectrum ( $\Gamma = 2.5$ ) still shows the back-scattering peak. As discussed at the end of §5, for column densities as high as  $10^{25} \text{ cm}^{-2}$ , two “rings” of emission on the surfaces of the torus that are parallel to the equatorial plane contribute flux to the Compton shoulder profile that has no forward or backward scattering preference. For flatter incident continua, the Fe  $K\alpha$  line photons are formed deeper in the medium because there are a relatively higher number of high-energy continuum photons (than in steeper spectra), which can penetrate deeper into the medium than lower energy photons. The higher energy continuum photons also undergo a larger number of mean scatterings than lower energy before being absorbed by an Fe K edge so that the resulting Fe  $K\alpha$  photons originate from a larger region. For these reasons Fe  $K\alpha$  photons that result from the absorption of high-energy continuum photons are more likely to scatter locally before escape, but the Fe  $K\alpha$  photons created by lower-energy continuum photons are more likely to encounter their first scattering on the far side of the torus. Therefore the Compton-shoulder has a relatively greater symmetric component for  $\Gamma = 1.5$  than for  $\Gamma = 2.5$ .

## 7 VELOCITY BROADENING

So far we have discussed the Compton shoulder profiles calculated directly from the Monte Carlo simulations, which do not include any kinematics. In practice, Doppler shifts due to bulk motion will broaden the Compton shoulders and such velocity broadening should be included when fitting real data with a model of the Fe  $K\alpha$  line. We also wish to study the possible confusion in velocity width measurements resulting from the doublet-splitting of the Fe  $K\alpha$  line. This is going to be especially important for observations of AGN made with calorimeters (as planned for *Astro-H*) which will have a spectral resolution for the Fe  $K\alpha$  line of several eV (for “local”, low-redshift AGN). For neutral Fe, the  $K\alpha$  emission consists of two lines,  $K\alpha_1$  at 6.404 keV and  $K\alpha_2$  at 6.391 keV, with a branching ratio of 2:1 (e.g. see Bambynek et al. 1972). In the Monte Carlo simulations these were treated as a single line with an energy of 6.4008 keV (corresponding to the weighted mean energies of the Fe  $K\alpha_1$  and Fe  $K\alpha_2$  lines). For the MYTORUS spectral-fitting model, the two components of the Fe  $K\alpha$  line are *reconstructed* using the above branching ratio and line energies. The energy difference between the two components is small enough to neglect the differences in opacities and the error incurred in this procedure is too small to impact fitting even *Astro-H* data. For each of the Fe line components,  $K\alpha_1$  and Fe  $K\alpha_2$ , we can construct a Compton shoulder for a given set of torus parameters, and sum the two profiles with the correct branching ratio. We then apply simple velocity broadening by convolving the summed profile with a Gaussian. The actual velocity-broadening function is *unlikely* to be a Gaussian, but it is also unlikely that even

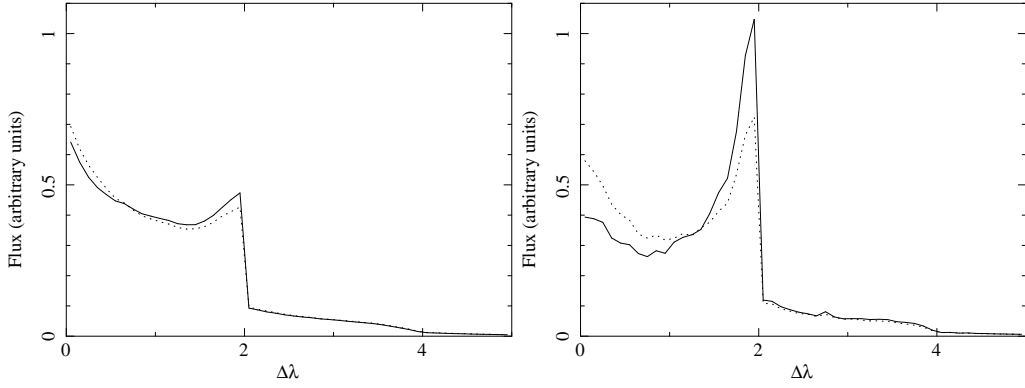


**Figure 5.** The Fe  $K\alpha$  emission-line Compton shoulders for  $N_{\text{H}} = 10^{25} \text{ cm}^{-2}$  and a power-law incident continuum with  $\Gamma = 1.5$  (dotted), and  $\Gamma = 2.5$  (solid). The *left-hand* panel corresponds to the face-on angle bin and the *right-hand* panel corresponds to the edge-on angle bin. No velocity broadening has been applied. Note that in order to directly compare the Compton shoulder shapes, the total flux for each shoulder has been renormalized to the same value. The line flux (in units of normalized flux per unit wavelength shift) is plotted against the Compton wavelength shift with respect to the zeroth-order rest-frame energy of the emission line ( $E_0$ ),  $\Delta\lambda = (511 \text{ keV}/E) - (511 \text{ keV}/E_0)$ .

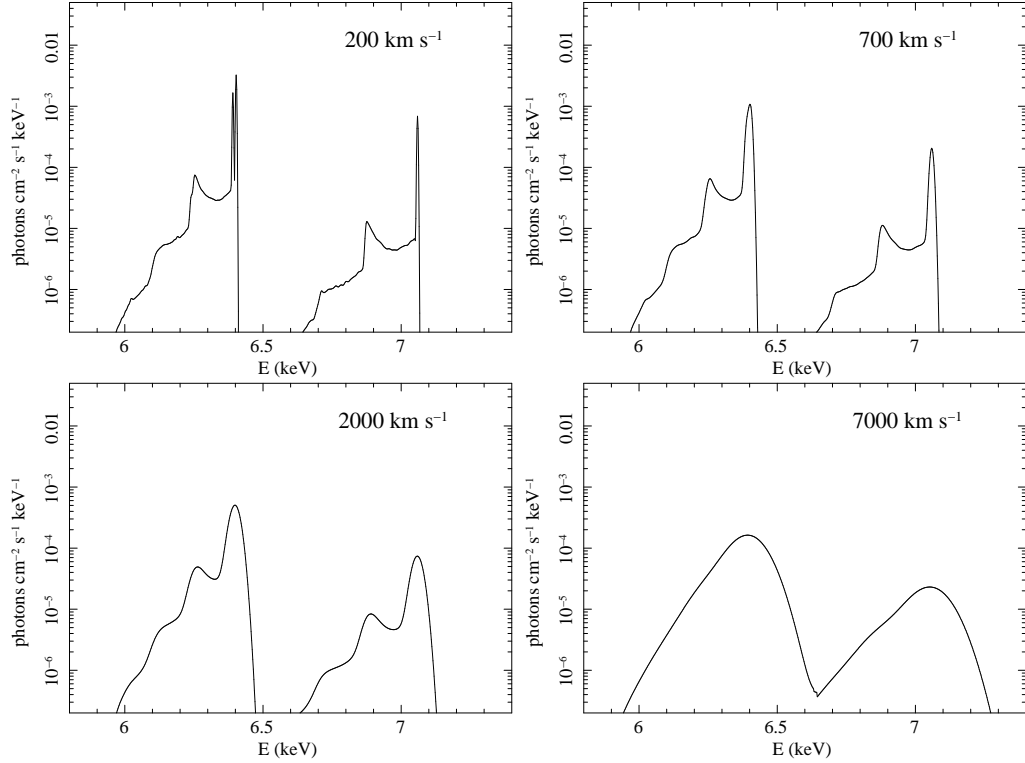


**Figure 6.** Effect of velocity broadening on the fluorescent emission-line spectra consisting of the Fe  $K\alpha_1$ , Fe  $K\alpha_2$ , and Fe  $K\beta$  lines. A Gaussian convolution function was applied to the Monte Carlo results for a toroidal X-ray reprocessor with  $N_{\text{H}} = 10^{25} \text{ cm}^{-2}$  (viewed *edge-on*), illuminated by a power-law continuum with a photon index of  $\Gamma = 1.9$ . Four emission-line spectra are shown with a FWHM of 200, 700, 2000, and 7000  $\text{km s}^{-1}$ . Note the logarithmic flux axis: the narrower core of the line for the smaller velocities makes the flux per keV in the core much higher than that in the Compton shoulder.

*Astro-H* will be able to distinguish between different geometries of the distant-matter Fe  $K\alpha$  line in AGN just from its velocity profile (e.g. see Yaqoob et al. 1993).

The effect of velocity broadening on the Fe  $K\alpha$  fluorescent line spectrum is illustrated in Fig. 6 for  $N_{\text{H}} = 10^{25} \text{ cm}^{-2}$  and the edge-on orientation (angle bin #10). This time we include the zeroth-order components of the emission lines, as well as the Compton shoulders, and we plot the spectra as a function of energy (and not  $\Delta\lambda$ ). We also show the Fe  $K\beta$  emission line which is also produced by our Monte Carlo simulations (see MY09 for details). A simple Gaussian function has been employed for convolving the emission-line profiles, using a FWHM velocity that is constant with respect to energy.

A total of four components are thus convolved (the zeroth-order components of Fe K $\alpha_1$  and Fe K $\alpha_2$ , and their respective Compton shoulders). Spectra are shown for four values of the FWHM, namely 200 km s $^{-1}$ , 700 km s $^{-1}$ , 2000 km s $^{-1}$ , and 7000 km s $^{-1}$ . The value of 200 km s $^{-1}$  is approximately the velocity resolution that will be achieved in the Fe K band by the calorimeters aboard *Astro-H*. The value of 700 km s $^{-1}$  is in the regime expected for the classical, parsec-scale torus. The value of 2000 km s $^{-1}$  is approximately the velocity resolution of the *Chandra* high energy grating (HEG) spectrometer in the Fe K energy band. It is also typical of optical emission-line widths in the outer BLR. The value of 7000 km s $^{-1}$  is approximately the velocity resolution of CCD detectors in the Fe K band. All emission-line spectra in Fig. 6 were calculated for an incident power-law spectrum with  $\Gamma = 1.9$ .

We see from Fig. 6 that the blending that results from velocity broadening can significantly dilute the characteristic features of the Compton shoulder and the combined Fe K $\alpha$  line profile. Notice that the zeroth-order cores for the Fe K $\alpha_1$  and Fe K $\alpha_2$  components cannot be distinguished as separate components even for a FWHM as low as 700 km s $^{-1}$  (this has already been pointed out in Yaqoob et al. 2001). At a FWHM of 2000 km s $^{-1}$  the Compton shoulder and line core are still resolved and the back-scattering peak is still resolved, although already heavily blended over the width of the shoulder. At a FWHM of 7000 km s $^{-1}$  there is no shoulder to the line profile and the only trace of it is a slight asymmetry in the line profile. An obvious implication of this is that *the Compton shoulder cannot be unambiguously resolved with CCD detectors*.

## 8 SUMMARY

We have studied the properties of the Compton shoulder of the Fe K $\alpha$  emission line in the toroidal X-ray reprocessor model of Murphy & Yaqoob (2009) for equatorial column densities in the range  $N_H = 10^{22}$  cm $^{-2}$  to  $10^{25}$  cm $^{-2}$  for the case of a half-opening angle of 60 $^\circ$  and the cosmic abundances of Anders & Grevesse (1989). The shape of the Compton shoulder and its flux relative to the core of the Fe K $\alpha$  emission line provide important physical constraints on the line-emitting matter, including column density and orientation of the reprocessing structure. We have made our results available in a form (the MYTORUS model) that is suitable for direct spectral-fitting to real, high spectral-resolution data.

We find that the ratio of the flux in the Compton shoulder to that in the unscattered core component of the Fe K $\alpha$  line increases approximately in proportion to  $N_H$  until  $N_H \sim 5 \times 10^{23}$  cm $^{-2}$ . The ratio reaches a maximum value that depends on the orientation of the torus ( $\sim 0.29$  for face-on and  $\sim 0.37$  edge-on), at  $N_H \sim 2 - 3 \times 10^{24}$  cm $^{-2}$ . The toroidal geometry gives a wider variety of Compton shoulder profiles than either (centrally-illuminated) spherical or disk geometries. When the torus is observed with non-intercepting lines-of-sight, the shape of the Compton shoulder of the Fe K $\alpha$  line as a function of Compton wavelength shift is approximately symmetrical over the wavelength interval corresponding to the first scattering. For intercepting lines-of-sight this symmetry is present in the optically-thin limit but the Compton shoulder profile becomes weighted more and more towards the zero wavelength shift side of the profile as the column density increases, even to only  $N_H \sim 10^{23}$  cm $^{-2}$ . The asymmetry continues to increase up to  $N_H \sim 2 - 3 \times 10^{24}$  cm $^{-2}$ . However, by  $N_H \sim 5 \times 10^{24}$  cm $^{-2}$  the Compton shoulder (in the first scattering interval) becomes symmetrical again.

Our Monte Carlo simulations have been performed with high statistical accuracy and reveal that the case of an edge-on, Compton-thick torus produces a new type of Compton shoulder that is unique to the toroidal geometry. It is dominated by a narrow back-scattering peak at  $\sim 6.24$  keV. In addition, our results are sensitive enough to reveal a weak dependence of the shape of the Compton shoulder and its magnitude (relative to the Fe K $\alpha$  line core), on the spectral shape of the incident X-ray continuum. We have also presented results on the effect of velocity broadening on the Fe K $\alpha$  line profile and find that if either the velocity width or instrument resolution is greater than a FWHM of  $\sim 2000$  km s $^{-1}$ , the Compton shoulder begins to become blended with the line core and the characteristic features of the Compton shoulder become harder to resolve. In particular, at a FWHM of 7000 km s $^{-1}$  the Compton shoulder is not resolved at all, its only signature being a weak asymmetry in the blended line profile. This means that CCD X-ray detectors cannot unambiguously resolve the Compton shoulder.

The properties of the Compton shoulder as a function of the torus opening angle (or covering factor) and the abundance of Fe cannot be trivially deduced and require much more extensive Monte Carlo simulations. This will be the subject of future work.

### Acknowledgments

Partial support (TY) for this work was provided by NASA through *Chandra* Award TM0-11009X, issued by the Chandra X-ray Observatory Center, which is operated by the Smithsonian Astrophysical Observatory for and on behalf of the NASA under contract NAS8-39073. Partial support from NASA grants NNX09AD01G and NNX10AE83G is also (TY) acknowledged.

## REFERENCES

- Anders E., Grevesse N., 1989, *Geochimica et Cosmochimica Acta* 53, 197  
 Bambynek W., Crasemann B., Fink R. W., Freund H.-U., Mark H., Swift C. D., Price R. E., Rao, P. V., 1972, *Rev. Mod. Phys.*, 44, 716

- Bianchi S., La Franca F., Matt G., Guainazzi M., Jiménez-Bailón E., Longinotti A. L., Nicastro F., Pentericci L., 2008, MNRAS, 389, L52
- Bianchi S., Matt G., Nicastro F., Porquet D., Dubau J., 2005, MNRAS, 357, 599
- Brightman M., Nandra K., 2008, MNRAS, 390, 1241
- Dorodnitsyn A., Kallman T., 2009, ApJ, 703, 1797
- Gaskell C. M., Goosmann R. W., Klimek E. S., 2008, MmSAI, 79, 1090
- George I. M., Fabian A. C., 1991, MNRAS, 249, 352
- Ghisellini G., Haardt F., Matt, G., 1994, MNRAS, 267, 743
- Ikeda S., Awaki H., Terashima, Y., 2009, ApJ, 692, 608
- Jiang P., Wang J. X., Wang T. G., 2006, ApJ, 644, 725
- Jiménez-Bailón E., Piconcelli E., Guainazzi M., Schartel N., Rodríguez-Pascual P. M., Santos-Lleó M., 2005, A&A, 435, 449
- Kallman T. R., Palmeri P., Bautista M. A., Mendoza C., Krolik J. H., 2004, ApJS, 155, 675
- Levenson N. A., Heckman T. M., Krolik J. H., Weaver K. A., Zycki P. T., 2006, ApJ, 648, 111
- Matt G., 2002, MNRAS, 337, 147
- Murphy K. D., Yaqoob T., 2009, MNRAS, 397, 1549 (MY09)
- Palmeri P., Mendoza C., Kallman T. R., Bautista M. A., Melendez M. 2003, A&A, 410, 359
- Reeves J. N., 2003, in *Active Galactic Nuclei: from Central Engine to Host Galaxy*, ed. S. Collin, F. Combes and I. Shlosman (Astronomical Society of the Pacific), Conference Series, Vol. 290, p. 35
- Shu X. W., Yaqoob T., Wang J. X., 2010, ApJS, 187, 581
- Sulentic J. W., Marziani P., Zwitter T., Calvani M., Dultzin-Hacyan D., 1998, ApJ, 501, 54
- Sunyaev R. A., Churazov E. M. 1996, *Astronomy Letters*, 22, 648
- Verner D. A., Ferland G. J., Korista K. T., Yakovlev D. G., 1996, ApJ, 465, 487
- Verner D. A., Yakovlev D. G., 1995 A&AS, 109, 125
- Watanabe S., Sako M., Ishida M. et al., 2003, ApJ, 597, 37
- Yaqoob, T., George I. M., Kallman T. R., Padmanabhan U., Weaver K. A., Turner T. J., 2003, ApJ, 596, 85
- Yaqoob T., George I. M., Nandra K., Turner T. J., Serlemitsos P. J., Mushotzky R. F., 2001, ApJ, 546, 759
- Yaqoob T., McKernan B., Done C., Serlemitsos P. J., Weaver K. A., 1993, ApJ, 416, L5
- Yaqoob T., Padmanabhan U., 2004, ApJ, 604, 63
- Zhou X. L., Wang J. M., 2005, ApJ, 618, L83